

Regulation of YAP by mTOR and autophagy reveals a therapeutic target of tuberous sclerosis complex

Ning Liang,^{1,2,3} Chi Zhang,^{1,2,3} Patricia Dill,^{1,2,3,4} Ganna Panasyuk,^{1,2,3} Delphine Pion,^{1,2,3} Vonda Koka,^{1,2,3} Morgan Gallazzini,^{1,2,3} Eric N. Olson,⁵ Hilaire Lam,⁶ Elizabeth P. Henske,⁶ Zheng Dong,⁷ Udayan Apte,⁸ Nicolas Pallet,^{9,10} Randy L. Johnson,¹¹ Fabiola Terzi,^{1,2,3} David J. Kwiatkowski,¹² Jean-Yves Scoazec,¹³ Guido Martignoni,^{14,15} and Mario Pende^{1,2,3}

¹Institut Necker-Enfants Malades, CS 61431, Paris, France

²Institut National de la Santé et de la Recherche Médicale, U1151, F-75014 Paris, France

³Université Paris Descartes, Sorbonne Paris Cité, 75006 Paris, France

⁴Department of Pediatric Neurology and Developmental Medicine, University Children's Hospital Basel, University of Basel, 4056 Basel, Switzerland

⁵Department of Molecular Biology, University of Texas Southwestern Medical Center, Dallas, TX 75390

⁶Pulmonary and Critical Care Medicine, Department of Medicine, Brigham and Women's Hospital, Harvard Medical School, Boston, MA 02115

⁷Department of Cellular Biology and Anatomy, Georgia Health Sciences University and Charlie Norwood VA Medical Center, Augusta, Georgia, GA 30192

⁸Department of Pharmacology, Toxicology and Therapeutics, University of Kansas Medical Center, Kansas City, KS 66160

⁹Institut National de la Santé et de la Recherche Médicale U775 and Université Paris Descartes, 75006 Paris, France

¹⁰Service de Néphrologie, Hôpital Européen Georges Pompidou, F-75015 Paris, France

¹¹Department of Biochemistry and Molecular Biology, University of Texas MD Anderson Cancer Center, Houston, Texas 77030

¹²Translational Medicine Division, Department of Medicine, Brigham and Women's Hospital, Harvard Medical School, Boston, MA 02115

¹³Hospices Civils de Lyon, Hôpital E. Herriot, 69437 Lyon, France

¹⁴Department of Pathology and Diagnostic, University of Verona, 37129 Verona, Italy

¹⁵Pederzoli Hospital, Peschiera, 37134 Verona, Italy

Genetic studies have shown that the tuberous sclerosis complex (TSC) 1–TSC2–mammalian target of Rapamycin (mTOR) and the Hippo–Yes–associated protein 1 (YAP) pathways are master regulators of organ size, which are often involved in tumorigenesis. The crosstalk between these signal transduction pathways in coordinating environmental cues, such as nutritional status and mechanical constraints, is crucial for tissue growth. Whether and how mTOR regulates YAP remains elusive. Here we describe a novel mouse model of TSC which develops renal mesenchymal lesions recapitulating human perivascular epithelioid cell tumors (PEComas) from patients with TSC. We identify that YAP is up-regulated by mTOR in mouse and human PEComas. YAP inhibition blunts abnormal proliferation and induces apoptosis of TSC1–TSC2–deficient cells, both in culture and in mosaic *Tsc1* mutant mice. We further delineate that YAP accumulation in TSC1/TSC2–deficient cells is due to impaired degradation of the protein by the autophagosome/lysosome system. Thus, the regulation of YAP by mTOR and autophagy is a novel mechanism of growth control, matching YAP activity with nutrient availability under growth-permissive conditions. YAP may serve as a potential therapeutic target for TSC and other diseases with dysregulated mTOR activity.

CORRESPONDENCE

Mario Pende:
mario.pende@inserm.fr

Abbreviations used: AML, angiomylipoma; CQ, chloroquine; mTOR, mammalian target of rapamycin; PEComa, perivascular epithelioid cell tumor; TSC, tuberous sclerosis complex; YAP, Yes-associated protein.

The tuberous sclerosis complex (TSC) is a genetic disease characterized by growth of hamartomas in different organs including brain, kidney, lung, skin, and heart (Crino et al., 2006). These lesions are a source of morbidity and mortality in patients with TSC, as they may cause intractable epilepsy, autism, developmental delay, renal, and pulmonary failure. Known causes

of TSC are loss of function mutations in *TSC1* and *TSC2* genes. The *TSC1* and *TSC2* gene products, together with a third subunit TBC1D7,

© 2014 Liang et al. This article is distributed under the terms of an Attribution–Noncommercial–Share Alike–No Mirror Sites license for the first six months after the publication date (see <http://www.rupress.org/terms>). After six months it is available under a Creative Commons License (Attribution–Noncommercial–Share Alike 3.0 Unported license, as described at <http://creativecommons.org/licenses/by-nc-sa/3.0/>).

form a ternary complex having GTPase activating protein (GAP) activity for the GTPase Rheb and therefore inhibiting mTOR complex 1 (mTORC1) kinase activity (Manning and Cantley, 2003; Dibble et al., 2012). The majority of TSC lesions contain multiple cell types of the mesenchymal lineage, as in the case of angiomyolipomas, lymphangioliomyomatosis, and angiofibromas. A unique cell type named perivascular epithelioid cell (PEC) is constantly present in mesenchymal TSC lesions, such as angiomyolipomas and lymphangioliomyomatosis, based on morphological features and the common expression of melanocytic and myogenic markers (Martignoni et al., 2008). Hence, these lesions are now officially classified, along with other tumors, as PEComas. Their cell of origin and the molecular mechanisms underlying their pathogenesis remain poorly defined.

TSC1/2–mTORC1 pathway senses and integrates a diversity of upstream signals, including growth factors, amino acids, oxygen, energy status, and stress, to control growth (Laplante and Sabatini, 2012). By phosphorylating specific effector proteins, mTORC1 up-regulates protein, RNA, DNA, glycogen, and lipid synthesis, as well as energy metabolism, including glycolysis and mitochondrial respiration. In addition, mTORC1 inhibits the initiation of autophagy, which is a eukaryotic catabolic pathway that sequesters cellular organelles and proteins in double-membrane autophagosomes, and delivers and degrades the cargos in lysosomes (He and Klionsky, 2009; Mizushima and Komatsu, 2011; Choi et al., 2013). Allosteric mTORC1 inhibitors, such as rapamycin derivatives, have been shown to be effective to the treatment of TSC lesions, including subependymal giant cell astrocytomas, angiomyolipomas, and lymphangioliomyomatosis (McCormack et al., 2011; Bissler et al., 2013; Franz et al., 2013). However, the tumors started regrowth when the treatment was discontinued. Moreover, the molecular nature underlying the regulation of abnormal proliferation and survival of TSC1/2–null cells downstream of mTORC1 remains to be fully understood.

In this study, we generated a mosaic *Tsc1* mutant mouse model that developed renal mesenchymal lesions showing similarities with human PEComas of TSC patients. To gain insights into the pathogenesis of these lesions, we screened the transcriptional outputs of several signaling pathways that govern proliferation, differentiation and maintenance of multipotency during development, including Notch, Wnt, Hedgehog, and Hippo pathways. Strikingly, we revealed a transcriptional signature of the Hippo pathway in *Tsc1* mutant kidneys. Hippo signaling pathway is a critical regulator of organ size during development, first identified in *Drosophila* and highly conserved in mammals (Pan, 2010; Halder and Johnson, 2011; Tapon and Harvey, 2012; Yu and Guan, 2013). Central to Hippo pathway is a kinase cascade composed of the Ste20-like protein kinase Hippo (MST1/2 in mammals) and the NDR family protein kinase Warts (Lats1/2 in mammals), disruption of which lead to tissue overgrowth and tumorigenesis in *Drosophila* and mice. Warts (Lats1/2 in mammals) kinase in turn phosphorylates and inactivates transcriptional co-activator Yorkie (YAP/TAZ in mammals), the downstream

effector of Hippo pathway. Yorkie and the mammalian orthologues YAP/TAZ have been reported to control proliferation, survival, epithelial to mesenchymal transition and multipotency, which may have oncogenic properties when their activity is not kept in balance (Huang et al., 2005; Camargo et al., 2007; Dong et al., 2007; Zhao et al., 2007, 2008; Brittle et al., 2010; Cordenonsi et al., 2011; Halder et al., 2012; Tumaneng et al., 2012; Calvo et al., 2013). We identified that YAP was up-regulated by mTOR in mouse and human TSC1/2–null cells. Inhibition of YAP, either genetically or pharmacologically, greatly attenuates the abnormal proliferation and induces apoptosis of TSC1/2–null cells, both in vitro and in PEComas of mosaic *Tsc1* mutant mice. Finally, we demonstrated that YAP accumulation in TSC1/2–deficient cells was due to impaired degradation of the protein by autophagy in a mTOR-dependent manner. These results suggested YAP as a potential therapeutic target for TSC and other diseases with dysregulated mTOR activity.

RESULTS

Generation of mosaic-*Tsc1*KO mice that develop multisystem lesions showing similarities with human TSC

Because TSC is a multiorgan mosaic disease with early manifestations in infancy and childhood, we generated mice that were homozygous for a floxed *Tsc1* allele (*Tsc1^{fl/fl}*), and carried a ubiquitously expressed and temporally regulated Cre transgenic allele (*CAGGCre-ERTM*; Hayashi and McMahon, 2002; Meikle et al., 2007). Depending on the dose of Tamoxifen (TM), Cre-ERTM stochastically causes recombination of floxed alleles in a variable percentage of cells in every tissue (Hayashi and McMahon, 2002), thus potentially targeting cells that give rise to the heterogeneous lesions. To circumvent the embryonic lethality of whole-body *Tsc1* deletion (Kobayashi et al., 2001), we injected a relatively low dose of TM (10 mg/kg) i.p. into pregnant dams at embryonic day 15.5 (E15.5). Cre-ERTM-positive pups were viable at birth and reached young adulthood at the same Mendelian frequency as the control littermates. However, the majority of Cre-ERTM-positive mice did not survive for longer than 10 wk. We therefore focused our analysis on 6-wk-old mice before the onset of lethality. At this age, recombination of the *Tsc1* allele was seen in every organ analyzed at 30–80% frequency, depending on the organ (Fig. 1 a). These data indicate that generalized mosaicism for complete *Tsc1* loss was achieved in these mice. Henceforth, these mutant mice shall be referred to as mosaic-*Tsc1*KO.

Histological analysis of mosaic-*Tsc1*KO mice was performed in multiple tissues, with special attention to anatomical locations that are commonly affected in TSC. The cerebral cortex revealed a disorganization of the cortical layers and the presence of enlarged dysplastic neurons immunoreactive with antibodies against phosphorylated ribosomal protein S6 (rpS6), a marker of mTORC1 activity (Fig. 1 b), as previously observed upon brain specific deletion of *Tsc1* (Meikle et al., 2007; Zhou et al., 2011). Furthermore, the dermal layer of the skin was thickened whereas the hypodermal fat

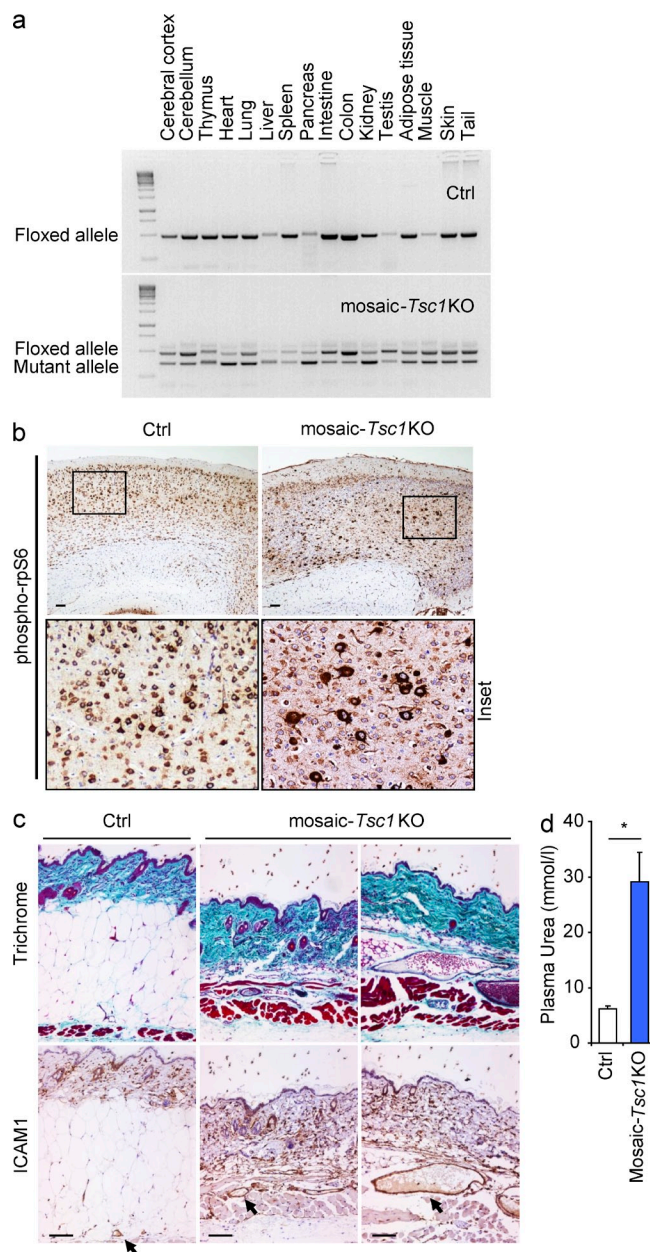


Figure 1. Mosaic-*Tsc1*KO mice develop multisystem lesions showing similarities with human TSC. (a) Genomic DNA was prepared from control (ctrl) and mosaic-*Tsc1*KO mice 1.5 mo after tamoxifen injection, and the floxed/mutant alleles were detected by PCR in the indicated organs. (b) Expression of phospho-rpS6 in cerebral cortex sections from ctrl and mosaic-*Tsc1*KO mice was analyzed by immunohistochemical staining. (c) Skin samples of ctrl and mosaic-*Tsc1*KO mice were stained for ICAM-1 expression and using Trichrome. Arrows indicate ICAM-1⁺ vessels. (d) Plasma urea concentrations were determined in ctrl and mosaic-*Tsc1*KO kidneys (Mean ± SEM; $n = 4$ mice/group; *, $P < 0.05$). Bars, 100 μ m. Three independent pregnant females were injected with tamoxifen. For immunohistochemistry analysis, similar stainings were found in four different ctrl/mosaic-*Tsc1*KO mice (6 wk of age, two sections per mouse).

layer was severely reduced, as assessed by Trichrome staining (Fig. 1 c). The vessels decorated by ICAM-1 antibodies were increased in numbers and abnormally enlarged in the dermal

and muscular layers of the skin of mosaic-*Tsc1*KO mice. Macroscopically, the fur of the mutant mice was fairer than in their littermates (unpublished data). Their kidneys were enlarged and highly susceptible to hemorrhage (Fig. 2 a). Kidney failure was underscored by a threefold increase of the plasma urea levels (Fig. 1 d). In conclusion, the mosaic-*Tsc1*KO mice develop a multisystem and early onset disease resembling different aspects of human TSC.

Mosaic-*Tsc1*KO mice develop renal mesenchymal lesions recapitulating PEComas associated with human TSC

We investigated whether the stochastic *Tsc1* deletion at E15.5 of embryogenesis target cells gives rise to mesenchymal lesions, such as PEComas. We examined the mutant kidneys in detail, as the observed hemorrhages might be caused by vascular lesions, and hemorrhage is an important complication of TSC renal angiomyolipoma (Bissler et al., 2013). Consistent with the phenotype in other TSC mutant animal models (Onda et al., 1999; Zhou et al., 2009), the mosaic-*Tsc1*KO kidneys were polycystic, a sign of abnormal proliferation of tubular epithelial cells (Fig. 2 b). However, immunostaining with Vimentin antibody, a marker of mesenchymal cells, revealed several lesions (Fig. 2 b), appearing as small, well defined, fasciculated nodules (Fig. 2 c). Cells within the lesions expressed additional mesenchymal markers, such as H-Caldesmon and α -smooth muscle actin (α SMA; Fig. 3, a and b). These nodules were proliferative, as demonstrated by immunostaining with Ki67 antibodies, and displayed high mTORC1 signaling, as shown by phosphorylation of rpS6 (Fig. 2 c). They were frequently observed near vessels (Fig. 2 c), and/or contained disorganized vascular components highlighted by CD31⁺ endothelial cells and PDGF receptor β - and α SMA-double positive pericytes (Fig. 3, a and b). Importantly, these mesenchymal lesions also showed immunoreactivity with the HMB45 antibody recognizing the melanocytic marker Pmel (also named gp100), which is a pathognomonic feature of PEComas (Fig. 2 d). Moreover, the mRNA levels of several melanocytic markers, including *Mart1*, *Cathepsin K*, *Pmel*, and *Tyrp1*, were sharply increased in mutant kidneys (Fig. 2 e). Finally, immunoblot analysis of protein extracts confirmed the induction of both melanocytic (*Mart1*) and myogenic (α SMA) markers, along with mTORC1 activation in mosaic-*Tsc1*KO kidneys (Fig. 2 f). To monitor Cre recombinase activity within the lesions, the mosaic-*Tsc1*KO mice were crossed with transgenic mice carrying a flox-stop-flox-lacZ reporter at the *Rosa26* locus. As shown in Fig. 3 c, the epithelial cells lining the cysts and the majority of the cells in the mesenchymal lesions underwent Cre-mediated recombination and were therefore *Tsc1* deficient.

To directly compare the mesenchymal lesions found in mosaic-*Tsc1*KO kidneys with human specimens, we screened samples of renal angiomyolipomas occurring in TSC patients. As shown in Fig. 2 g, the majority of human angiomyolipomas were surrounded by several smaller lesions, so called microhamartomas (or microscopic angiomyolipomas), which shared the common expression of *cathepsin K*, α -SMA, and

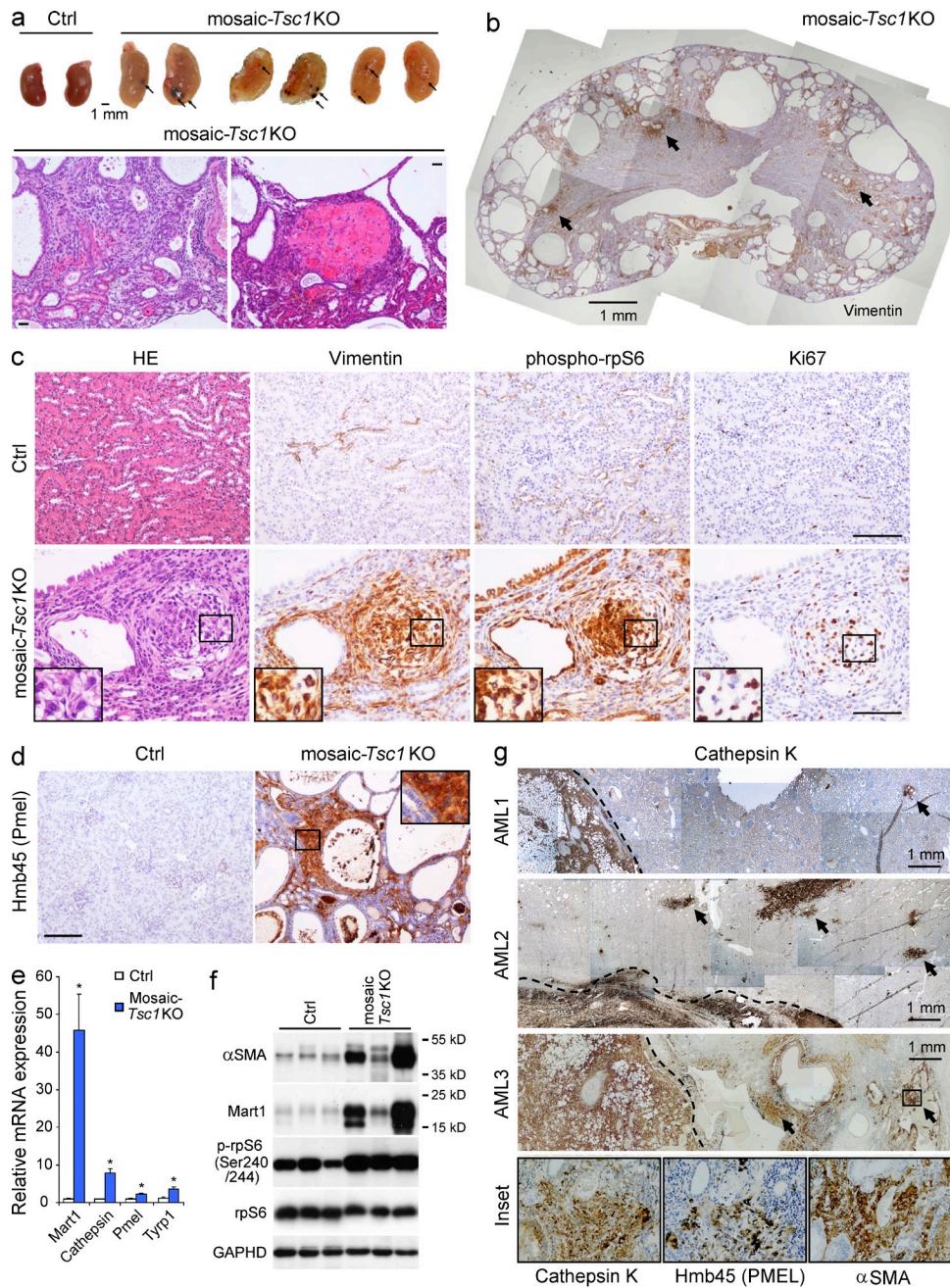


Figure 2. Mosaic-*Tsc1*KO mice develop renal mesenchymal lesions recapitulating PEComas associated with human TSC. Kidneys from ctrl ($n = 3$) and mosaic-*Tsc1*KO ($n = 3$) mice were analyzed at 6 wk of age. (a) Macroscopic photos and representative H&E staining. Arrows indicate hemorrhages. (b–d) Expression of vimentin (b and c), phospho-rpS6, and Ki67 (c) and Hmb45/Pmel (d) was assessed by immunohistochemistry. H&E staining was shown on left in c. Arrows in b indicate vimentin⁺ microhamartomas in mosaic-*Tsc1*KO kidneys. For immunohistochemistry analysis, similar stainings were found in three different ctrl/mosaic-*Tsc1*KO mice (three sections per mouse). (e) Expression of Mart1, Cathepsin K, Pmel, and Tyrp1 mRNA was assessed by qRT-PCR. Mean \pm SEM; $n = 3$ mice/group; *, $P < 0.05$. (f) Expression of α -SMA, Mart1, p-rpS6, and total rpS6 protein was assessed by Immunoblot. (g) Expression of the indicated proteins in three distinct human angiomyolipoma (AML) samples was assessed by immunohistochemistry. Arrows indicate the microhamartoma. Bar, 100 μ m unless otherwise indicated. Insets show higher magnification of the lesions indicated with squares.

Pmel. It is likely that the small lesions represent early developmental stage of angiomyolipomas. Importantly, these microhamartomas exhibited a striking similarity with their murine counterparts in terms of morphology and immunophenotype. In conclusion, mosaic-*Tsc1*KO mouse kidneys develop renal

mesenchymal lesions similar to the PEComas observed in human TSC patients. However, we did not observe any kidney angiomyolipomas in these mice. This may be because of the premature mortality seen in these mice, precluding further lesion development into full blown angiomyolipomas.

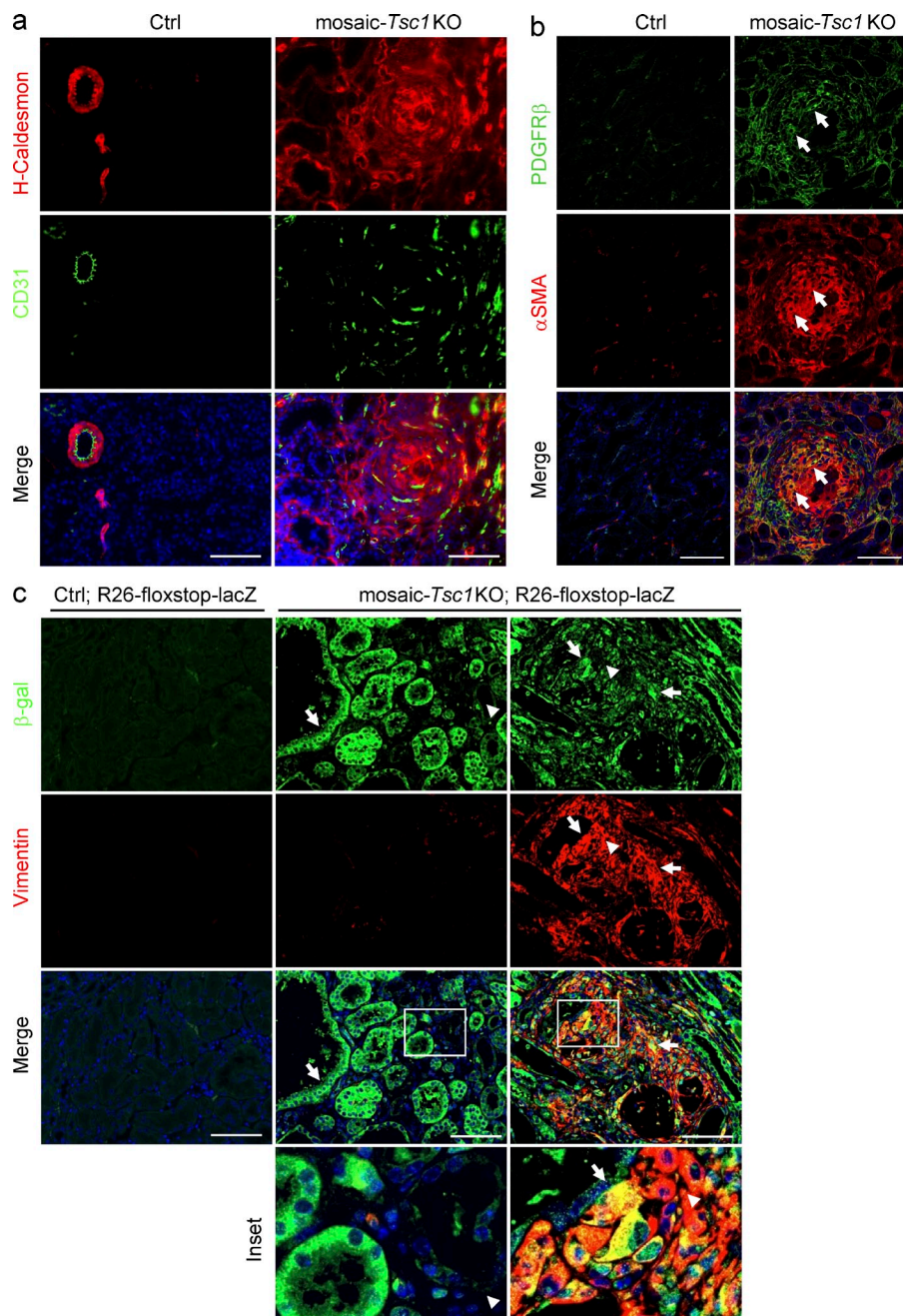


Figure 3. Mosaic-*Tsc1*KO mice develop renal H-caldesmon⁺ mesenchymal lesions containing CD31⁺ endothelial cells and PDGFRβ⁺/αSMA⁺ pericytes. (a and b) Kidney tissues were isolated from ctrl and mosaic-*Tsc1*KO mice at 6 wk of age and analyzed by immunofluorescence for H-caldesmon and CD31 (a) or PDGFRβ and αSMA (b). Arrows in b indicate PDGFRβ- and αSMA-double-positive pericytes. (c) Expression of β-gal and vimentin on kidney sections from Ctrl; R26-floxstop-LacZ and mosaic-*Tsc1*KO;R26-floxstop-LacZ mice was assessed by immunofluorescence. Arrows indicate β-gal⁺ cells and arrowheads show β-gal⁻ cells. Insets show higher magnification of tissue indicated with squares. Similar stainings were found in three different mice/genotype (three sections per each mouse). Bars: (A–C) 100 μm.

YAP is up-regulated by mTOR in renal lesions of mosaic-*Tsc1*KO mice and human angiomyolipoma

The phenotype of mosaic-*Tsc1*KO mouse kidneys consisted of enlarged organ size, polycystosis, and microscopic PEComas. To gain mechanistic insights, we screened transcriptional outputs of developmental pathways involved in tissue growth, planar cell polarity, and multipotency. These included target genes of Notch, Wnt, Hedgehog, and Hippo pathways (Fig. 4 a and not depicted). The mosaic-*Tsc1*KO kidneys had a two- to eightfold increase in mRNA levels of connective tissue growth factor (CTGF), amphiregulin (Areg), and Cyr61, all known

transcriptional targets of the Hippo pathway (Tumaneng et al., 2012). This stimulation was blunted by treating the mice every other day for 2 wk with the rapamycin derivative temsirolimus (5 mg/kg), suggesting a tight control of the Hippo pathway by mTOR in *Tsc1* mutant kidneys. Next, we examined the levels of YAP, whose function is required for the transcriptional regulation of CTGF, Areg, and Cyr61 downstream of the Hippo pathway. Whereas YAP mRNA levels were not affected by *Tsc1* deletion and mTOR inhibition (Fig. 4 a), the protein amount was tightly correlated with mTORC1 activity as assessed by phosphorylated rpS6 levels in kidneys (Fig. 4 b). The increase in

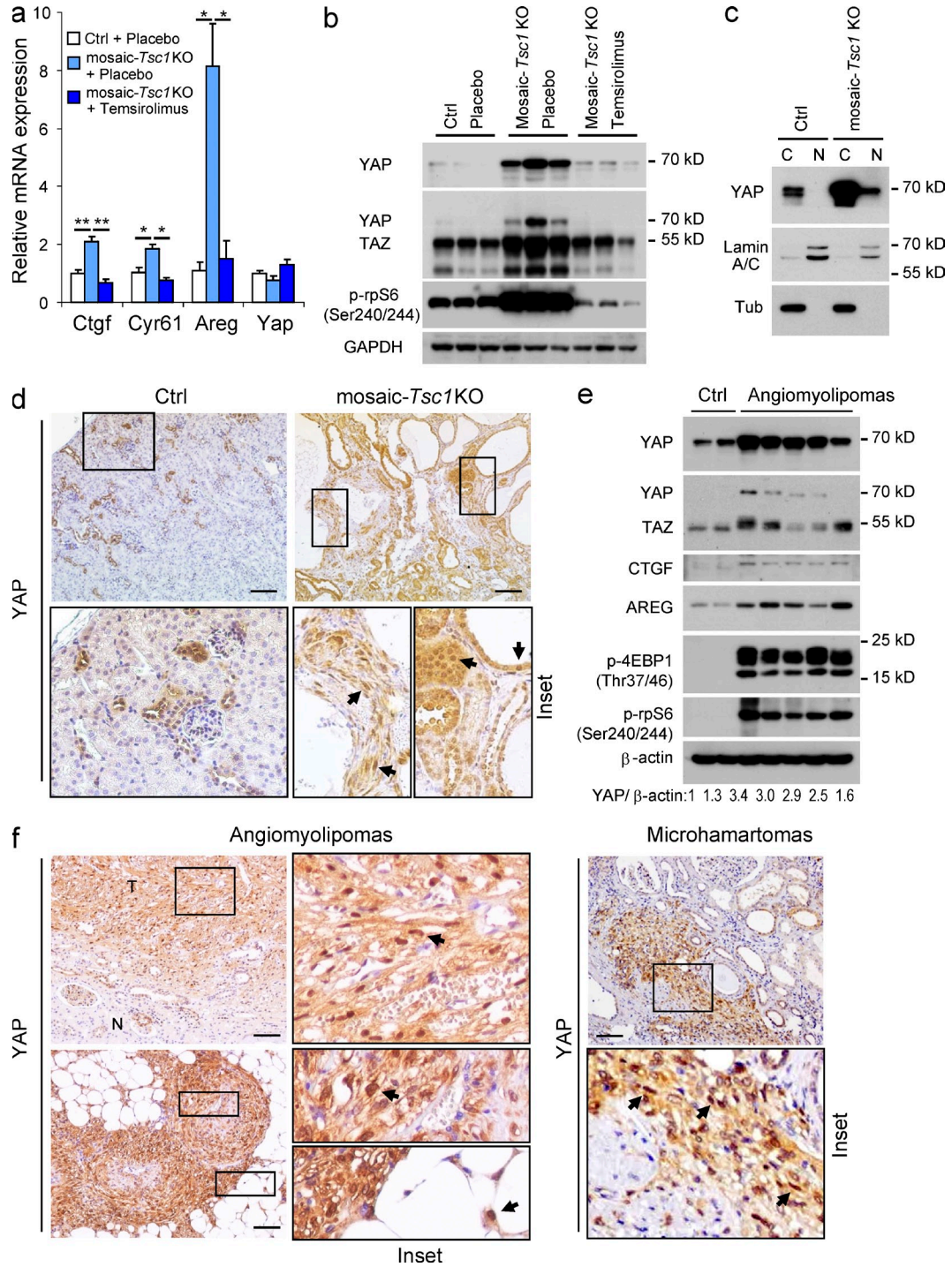


Figure 4. YAP is up-regulated by mTOR in renal lesions of mosaic-Tsc1KO mice and human angiomyolipoma. (a and b) Expression of indicated genes was determined by qRT-PCR (a) and immunoblot analysis (b) in kidney samples from Ctrl mice treated with placebo, mosaic-Tsc1KO mice treated with placebo, or temsirolimus. Mice were injected i.p. with vehicle or temsirolimus (5 mg/kg) every other day for 2 wk before sacrifice. Mice were sacrificed at 6 wk of age. Mean \pm SEM; $n = 3$ mice/group; *, $P < 0.05$, **, $P < 0.01$. (c) Expression of indicated proteins was analyzed by immunoblot in nuclear and cytoplasmic protein extractions from ctrl and mosaic-Tsc1KO mouse kidney samples. Similar results were found in three different mice/genotype. (d) YAP expression was assessed on kidney sections from ctrl and mosaic-Tsc1KO mice by immunohistochemistry. Arrows indicate cells with YAP nuclear localization. Bars, 100 μ m. Similar stainings were found in three different mice/genotype (three sections per each mouse). (e) Expression of indicated proteins was analyzed by immunoblot in control human kidney and angiomyolipoma samples. (f and g) YAP expression was analyzed by immunohistochemistry on human angiomyolipoma samples (N, normal kidney; T, Tumor). Arrows indicate cells with YAP nuclear localization. Bars, 100 μ m. Insets show higher magnification of the lesions indicated with squares. Similar results were found in 7/7 different human angiomyolipoma samples.

YAP levels was detected both in cytosol and nuclei (Fig. 4 c). TAZ, the homologue of YAP, was also up-regulated at the protein level in mosaic-*Tsc1*KO kidneys (Fig. 4 b).

To localize the kidney cell compartment expressing YAP, immunostaining was performed (Fig. 4 d). In adult floxed control littermates, YAP was found in scattered tubular epithelial cells of the kidney cortex. Strikingly, *Tsc1* deletion caused a widespread expression of YAP in both tubular epithelial cells lining the cysts and in spindle-shaped mesenchymal cells of the kidney cortex. Notably, in the mosaic-*Tsc1*KO mouse kidneys, a large fraction of YAP was localized in the nuclei, consistent with an active function as a transcriptional regulator.

To determine whether the activation of the YAP pathway also occurred in human TSC, first we examined YAP, CTGF, and Areg protein levels in TSC angiomyolipomas by immunoblotting (Fig. 4 e). The activation of mTORC1, as assessed by 4EBP1 and rpS6 phosphorylation, and the increased YAP protein were seen in all samples examined. Importantly, the transcriptional targets CTGF and Areg were also expressed at higher levels in angiomyolipomas. Because the levels of TAZ were more variable among the human samples analyzed, we decided to focus our analysis on YAP in this study. Next, we analyzed YAP localization in the different cell types of human angiomyolipomas and in the adjacent kidney structures. As shown in Fig. 4 f, high levels of YAP immunoreactivity were detected in all cell types that could be found in angiomyolipomas, i.e., adipocytes, smooth muscle cells, and blood vessel components. In the adjacent kidney regions, YAP protein was almost undetectable, except for small YAP-positive cysts of epithelial origin lining the lesion. The YAP antibody also stained small human renal micro-hamartomas that closely resembled the mesenchymal lesions observed in mosaic-*Tsc1*KO mouse kidneys (Fig. 4 g). Finally, we examined other human TSC-related PEComas from different organs. In pulmonary lymphangiomyomatosis, hepatic angiomyolipomas, as in renal angiomyolipomas, YAP expression invariably correlated with mTORC1 activity in tumor cells (unpublished data). After screening a total of 10 PEComas, YAP was found to be consistently highly expressed in all the specimens and can be considered a novel marker. Interestingly, we detect YAP expression already at early stages of human PEComa development, suggesting a putative role in the origin of the lesion.

YAP is required for the abnormal proliferation and survival of TSC1/2-null cells in vitro

We then examined whether YAP contributed to the growth phenotype of TSC1/TSC2-deficient cells. We cultured mouse embryonic fibroblasts (MEFs) that were *Tsc2*^{-/-} and *Tsc2*^{+/+} MEFs, which were in *p53*^{-/-} background (Zhang et al., 2003). YAP protein levels were increased by threefold in the *Tsc2*-null cells (Fig. 5 a). This effect was also observed in nuclear fractions (not depicted), and was paralleled by increased expression of the YAP target CTGF (Fig. 5, a and g). Thus, the up-regulation of the YAP pathway can also be observed in a cell-autonomous manner upon TSC complex deficiency. This effect could not be ascribed to a relief of Hippo/Lats inhibition

of YAP in *Tsc2*-null cells, because the amount of Ser112-phosphorylated YAP, a site of the Lats1/2 kinases (Zhao et al., 2010), paralleled the increase in total YAP protein in the mutant cells (Fig. 5 a). *Tsc2* deletion is known to provide a proliferative advantage over wild-type controls in serum starvation conditions (Zhang et al., 2003). After 24 h of serum starvation, the phosphorylation of the mTORC1 substrate rpS6 and the YAP protein levels were shut off in controls, while remaining high in *Tsc2*^{-/-} cells (Fig. 5 b). As expected, cell counting over a 3-d period after serum starvation indicated that the number of *Tsc2*^{-/-} cells steadily increased as opposed to wild type control (Fig. 5 c). Importantly, the proliferation of *Tsc2*^{-/-} cells was blunted by YAP knockdown (Fig. 5, c and d). Cell viability was also sensitive to YAP levels, as indicated by the drop in cell number at the 72-h time point (Fig. 5 c), and the increase in TUNEL⁺ apoptotic cells (Fig. 5 e). The effect of YAP knockdown was mimicked by treatment with verteporfin, a compound that was reported to interfere with YAP binding to the TEAD1-4 transcription factors, and accordingly inhibited CTGF mRNA expression in *Tsc2*^{-/-} cells (Fig. 5, f and g; Liu-Chittenden et al., 2012). YAP levels were also increased after TSC1 and TSC2 knockdown by RNAi in human embryonic kidney 293 (HEK293) cells (Fig. 5 h). The concomitant knockdown of YAP impaired the proliferative advantage of TSC1-depleted HEK293 cells in serum-starved conditions (Fig. 5 i). Collectively, these data demonstrate that YAP activity is, at least partly, required to promote proliferation of TSC complex-deficient cells in vitro.

Inhibition of YAP pharmacologically or genetically attenuates abnormal proliferation and induces apoptosis of *Tsc1*-null cells in vivo

To assess the effects of YAP inhibition in vivo, mosaic-*Tsc1*KO and control mice were treated i.p. with verteporfin (100 mg/kg) every other day for 10 d (Liu-Chittenden et al., 2012). The YAP inhibitor reduced the kidney/body weight ratio by 50% (Fig. 6 a), and attenuated overall kidney size and polycystosis in mutant mice without affecting control kidneys (Fig. 6 b). These effects were concomitant to a reduction in CTGF expression (Fig. 6 c). The proliferation of the mesenchymal lesions was severely affected by verteporfin treatment, as indicated by Ki67 staining of α -SMA⁺ cells (Fig. 6 d). Furthermore, verteporfin treatment led to apoptosis of both epithelial and mesenchymal cells in mosaic-*Tsc1*KO kidneys (Fig. 6 e). To specifically affect YAP expression by genetic means, we crossed *CAGGCre-ER*TM; *Tsc1*^{f/f} with *Tsc1*^{f/f}; *Yap*^{f/+} mice. The offspring mice were injected with TM at postnatal day 2 (P2), to generate mosaic-*Tsc1*KO carrying a mutant allele of *Yap* (mosaic-*Tsc1*KO; *Yap*^{+/-}). The heterozygous deletion of *Yap* was sufficient to reduce YAP protein levels in mosaic-*Tsc1*KO mice (Fig. 7 c). This was accompanied by a sharp attenuation of the kidney phenotype as compared with mosaic-*Tsc1*KO mice, as assessed by the kidney to body weight ratio (Fig. 7 a), kidney size and polycystosis (Fig. 7 b), and mesenchymal cell proliferation (Fig. 7, d and e). The

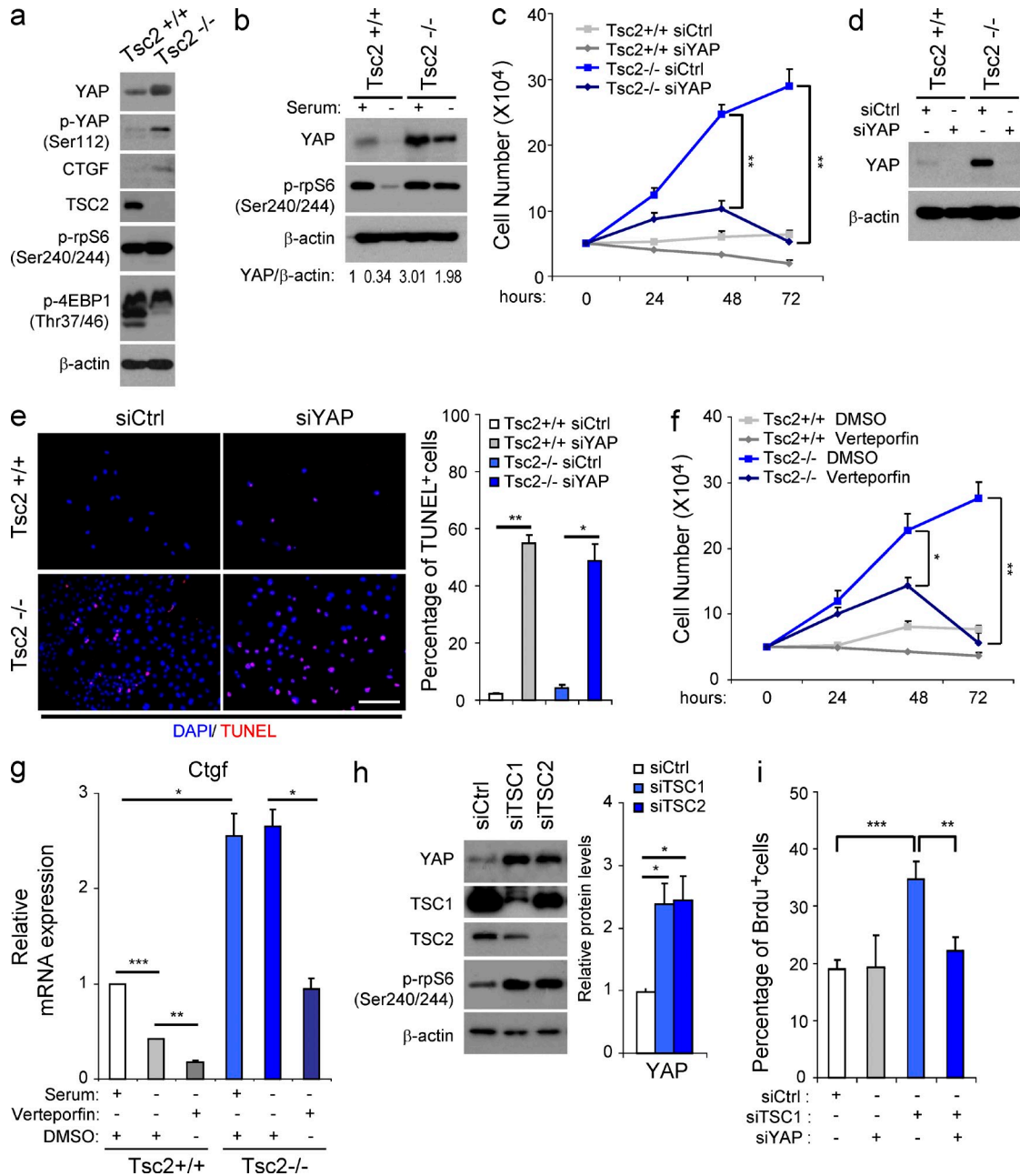


Figure 5. YAP is required for the abnormal proliferation and survival of TSC1/2-null cells in vitro. (a and b) Expression of indicated proteins was analyzed by immunoblot in *Tsc2*^{+/+} and *Tsc2*^{-/-} MEFs (these MEFs were generated in *p53*^{-/-} background) cultured with or without serum for 24 h. Similar results were observed in three independent experiments. (c–e) *Tsc2*^{+/+} and *Tsc2*^{-/-} MEFs transfected with siCtrl or siYAP were cultured in serum starvation conditions for a 72-h period. (c) Cell number was counted in different groups. Three independent experiments were performed and analyzed (Mean ± SEM; **, *P* < 0.01). (d) Expression of YAP protein was analyzed by immunoblot at the 24-h time point. Similar results were observed in three independent experiments. (e) Apoptotic cells were identified by TUNEL assay at the 48-h time point. The percentage of TUNEL⁺ cells was determined by counting TUNEL⁺ nuclei among at least 500 cells in distinct fields of each experiment. Three independent experiments were performed and analyzed. Mean ± SEM; *, *P* < 0.05, **, *P* < 0.01. (f and g) *Tsc2*^{+/+} and *Tsc2*^{-/-} MEFs were cultured under serum starvation conditions and treated with DMSO or Verteporfin for a 72-h period. (f) Cell number was counted. Three independent experiments were performed and analyzed. Mean ± SEM; *, *P* < 0.05, **, *P* < 0.01. (g) Expression of *Ctgf* mRNA was assessed by qRT-PCR in different treatments. Three independent experiments were performed and analyzed. Mean ± SEM; *, *P* < 0.05, **, *P* < 0.01, ***, *P* < 0.001. (h) Expression of indicated proteins was analyzed by immunoblot in HEK293 cells transfected with siRNAs against TSC1, TSC2, or siCtrl. YAP protein level was normalized with β-actin. Four independent experiments were performed and analyzed. Mean ± SEM; *, *P* < 0.05. (i) Percentage of BrdU⁺ HEK293 cells with indicated treatments under serum deprivation conditions for 24 h was assessed by 3-h BrdU pulse-labeling before harvest. Three independent experiments were performed and analyzed. Mean ± SEM; **, *P* < 0.01, ***, *P* < 0.001.

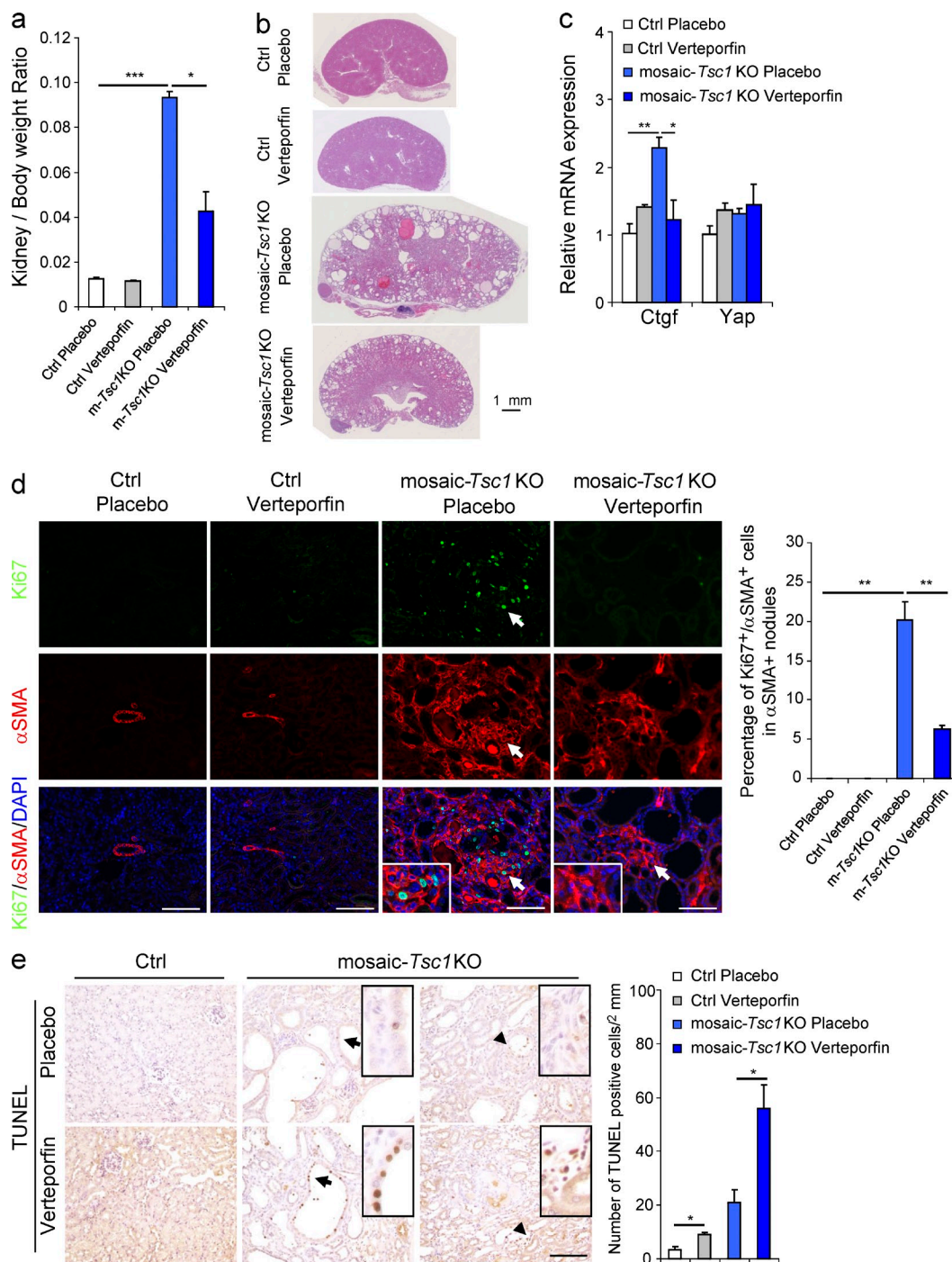


Figure 6. Verteporfin treatment inhibits proliferation and induces apoptosis of *Tsc1*-null cells in vivo. Mice were administered i.p. with vehicle or verteporfin at a dose of 100 mg/kg every other day for 10 d before sacrifice. Mice were sacrificed at 6 wk of age. Three independent experiments were performed and mice in different treatments were pooled for analysis. (a) Kidney/body weight ratio of Ctrl and mosaic-*Tsc1* KO mice treated with placebo or Verteporfin. $n = 3$ mice/group. Mean \pm SEM; *, $P < 0.05$, ***, $P < 0.001$. (b) Representative pictures of hematoxylin and eosin staining of kidney sections from Ctrl and mosaic-*Tsc1* KO mice treated with placebo or Verteporfin. Bar, 1 mm. (c) Expression of indicated mRNAs was analyzed by qRT-PCR in kidney samples from Ctrl and mosaic-*Tsc1* KO mice treated with placebo or Verteporfin. $n = 3$ mice/group. Mean \pm SEM; *, $P < 0.05$, **, $P < 0.01$. (d) Percentage of Ki67 and α SMA double-positive cells in α SMA+ mesenchymal lesions in the indicated kidneys. Immunofluorescence staining and counting were performed on three sagittal sections from different kidney regions for each mouse. Representative images are shown. Mean \pm SEM; $n = 3$ mice/group; **, $P < 0.01$; Bar, 100 μ m. Insets show the lesions indicated with arrows. (e) In situ apoptotic cells were assessed by TUNEL assay on the kidney sections from Ctrl and mosaic-*Tsc1* KO mice treated with placebo or verteporfin. The number of TUNEL+ cells were counted in ten distinct fields of each section. Three sections were analyzed per each mouse. Representative images are shown. Arrows indicate TUNEL+ epithelial cells and arrowheads show TUNEL+ mesenchymal cells. Insets show the lesions indicated with arrows. Mean \pm SEM; $n = 3$ mice/group; *, $P < 0.05$; Bar 100 μ m.

residual lesions observed in mosaic-*Tsc1*KO;*Yap*^{+/-} kidneys displayed rpS6 phosphorylation, suggesting efficient recombination (unpublished data). Whole-body heterozygous deletion of *Yap* (*Yap*^{+/-}) did not inhibit kidney growth and proliferation (Fig. 7, f-h), indicating that the reduction of YAP gene dosage was particularly effective in a background of *Tsc1* loss of function. Thus, strategies targeting YAP activity might

be beneficial in treating TSC-related kidney overgrowth and PEComa formation.

YAP is accumulated in TSC-deficient cells due to blockage of autophagy in a mTOR-dependent manner

YAP is under the tight control of a variety of upstream regulators (Tumaneng et al., 2012). To gain mechanistic insights

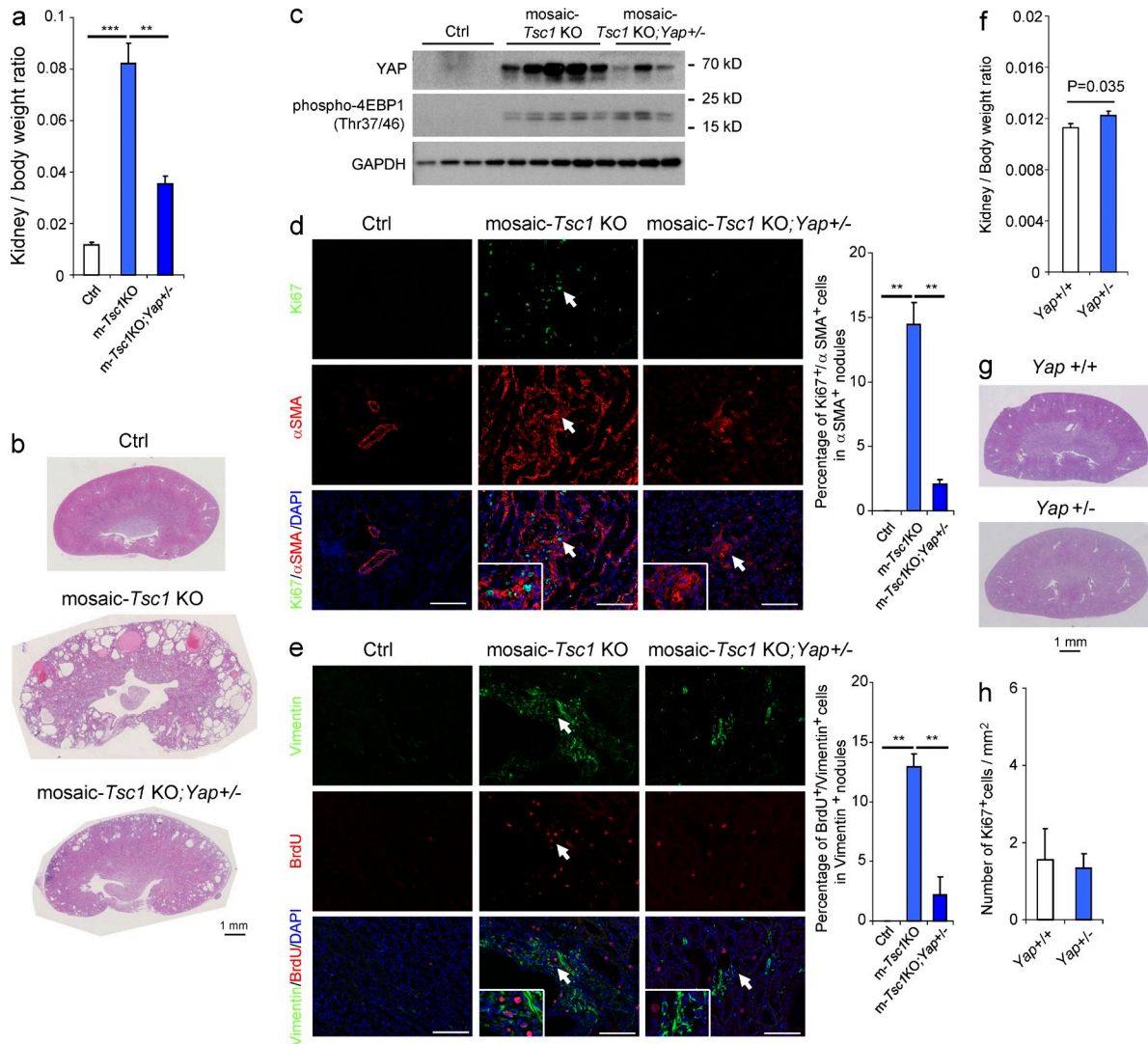


Figure 7. Heterozygous deletion of Yap compromises the proliferation of renal mesenchymal lesions in mosaic-*Tsc1*KO mice. Three independent tamoxifen injection experiments were performed and female mice of indicated genotypes were pooled for analysis. (a) Kidney/body weight ratio of the indicated mice sacrificed at 6 wk of age (Ctrl, *n* = 4; mosaic-*Tsc1*KO, *n* = 5; mosaic-*Tsc1*KO;*Yap*^{+/-}, *n* = 3). (b) Representative pictures of hematoxylin and eosin staining of kidney sections from the indicated mice. (c) Expression of indicated proteins was analyzed by immunoblot in mouse kidney samples from the indicated genotypes. (d) Percentage of Ki67 and α-SMA double-positive cells in α-SMA⁺ kidney lesions from mice of the indicated genotypes. Immunofluorescence staining and counting were performed on three sagittal sections from different kidney regions for each mouse (Ctrl, *n* = 4; mosaic-*Tsc1*KO, *n* = 5; mosaic-*Tsc1*KO;*Yap*^{+/-}, *n* = 3). Insets show the lesions indicated with arrows. Bars, 100 μm. Mean ± SEM, **, *P* < 0.01. (e) Percentage of BrdU and Vimentin double-positive cells in Vimentin⁺ mesenchymal lesions in the indicated kidneys. BrdU (50 mg/kg) was injected i.p. 24 h before sacrifice. Immunofluorescence staining and counting were performed on three sagittal sections from different kidney regions for each mouse. Representative images are shown (Ctrl, *n* = 4; mosaic-*Tsc1*KO, *n* = 5; mosaic-*Tsc1*KO;*Yap*^{+/-}, *n* = 3; mean ± SEM; **, *P* < 0.01; Bar, 100 μm). Insets show the lesions indicated with arrows. (f) Kidney/body weight ratio of *Yap*^{+/+} (*n* = 3) and *Yap*^{+/-} (*n* = 3) mice. (g) Hematoxylin and eosin staining of kidney sections from *Yap*^{+/+} and *Yap*^{+/-} mice. Bar, 1 mm. (h) Percentage of Ki67⁺ cells per mm² in kidney sections from *Yap*^{+/+} and *Yap*^{+/-} mice (*n* = 3). The number of Ki67⁺ cells were counted in 10 distinct fields per each section. Two sections were analyzed per each mouse.

into the novel crosstalk between the TSC1/TSC2/mTORC1 and YAP, we asked which step of YAP expression was affected in *Tsc2*^{-/-} cells. Consistent with the data in mosaic-*Tsc1*KO kidneys (Fig. 4 a), the comparable YAP mRNA amount in *Tsc2*^{-/-} and *Tsc2*^{+/+} cells ruled out transcriptional effects (unpublished data). We did not find evidence for a regulation at the step of translational initiation, as the recruitment of YAP mRNA in the polysomal fraction was also equivalent in the two genotypes (unpublished data). A major node in YAP regulation is the phosphorylation on five serine

residues by the Lats1/2 kinases that causes cytosolic retention and promotes protein degradation by the proteasome (Huang et al., 2005; Zhao et al., 2010). However, no major alteration in Lats1/2 kinase activity was detected in *Tsc2*^{-/-} cells and kidney tissues, as indicated by the Ser-112 YAP phosphorylation (Fig. 5 a and not depicted). Accordingly, 8-h treatment with the proteasome inhibitor MG132, while leading to a significant accumulation of polyubiquitinated proteins, did not affect YAP levels in either *Tsc2*^{-/-} or control cells in growing conditions (unpublished data). Intriguingly, the YAP

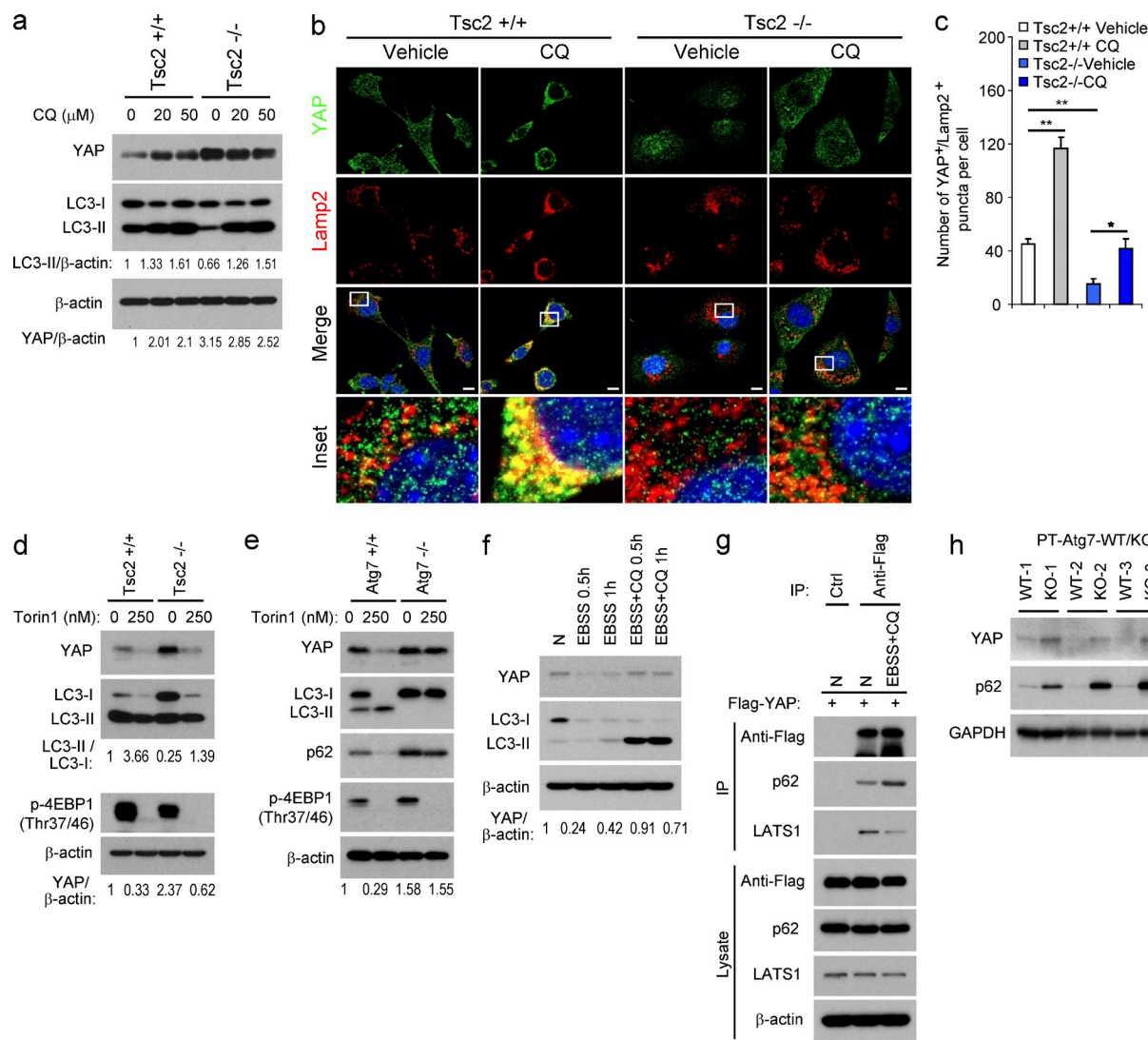


Figure 8. YAP is accumulated in TSC deficient cells due to blockage of autophagy. (a) Expression of indicated proteins was analyzed by immunoblot in *Tsc2*^{+/+} and *Tsc2*^{-/-} MEFs treated with or without chloroquine (CQ) for 8 h. Similar results were observed in three independent experiments. (b, c) Localization of YAP and Lamp2 was analyzed by immunofluorescence in *Tsc2*^{+/+} and *Tsc2*^{-/-} MEFs treated with or without CQ (20 μM) for 24 h. Insets show part of the cells indicated with squares. 50 cells were counted for yellow punctas in each group. Three independent experiments were performed and analyzed (mean ± SEM; *, P < 0.05, **, P < 0.01; Bar 10 μm). (d and e) Expression of indicated proteins was analyzed by immunoblot in *Tsc2*^{+/+}, *Tsc2*^{-/-} and *Atg7*^{+/+}, *Atg7*^{-/-} MEFs culturing with or without Torin1 for 24 h. Similar results were observed in three independent experiments. (f) Immunoblot analysis of YAP and LC3 in HeLa cells with indicated treatments. YAP levels were normalized with β-actin. Similar results were observed in three independent experiments. (g) Immunoprecipitation analysis of interacting proteins of flag-tagged YAP in the indicated culturing conditions for 0.5 h. Similar results were observed in three independent experiments. (h) Expression of indicated proteins was analyzed by immunoblot in ctrl (n = 3) and proximal tubule-specific *Atg7* knockout mouse kidney samples (n = 3).

phosphorylation by Lats1/2 kinases has been reported to induce a rapid degradation of YAP in high- but not low-density culture conditions (Zhao et al., 2010), the latter pertaining to the experimental setup used in this study. Thus, in growing cells with no contact inhibition and with high mTOR activity, YAP levels are controlled by an alternative mechanism.

TSC1/2 mutant cells have impaired autophagic flux (Parkhitko et al., 2011; Dibble et al., 2012), as indicated by the reduced conversion of LC3-I to the cleaved and lipidated form LC3-II (Fig. 8 c). We wondered whether an alteration in the lysosomal route of degradation might explain the YAP accumulation in *Tsc2*^{-/-} MEFs. The lysosomotropic drug and autophagy inhibitor chloroquine (CQ) led to the accumulation of LC3-II that normally undergoes lysosomal turnover. This effect was paralleled by the accumulation of YAP protein in control MEFs, whereas the amount of YAP was not further increased by chloroquine in *Tsc2*^{-/-} cells (Fig. 8 a). In MEFs, YAP protein was localized in cytosol, nucleus, and cytosolic vesicles, a fraction of which was also positive for the lysosomal marker Lamp2 (Fig. 8 b). Impairment of lysosomal degradation by chloroquine treatment increased the amount of YAP detectable in the lysosomes, indicating that YAP is a cargo for lysosomal degradation. In *Tsc2*^{-/-} cells, the amount of YAP localized in the lysosomes was reduced as compared with control cells in both untreated and chloroquine-treated conditions (Fig. 8, b and c). Notably, interactome studies in *Drosophila* cells revealed a strong association of the Hippo pathway with endocytosis and vesicle-trafficking complexes (Kwon et al., 2013).

To analyze the crosstalk between mTOR kinase activity and YAP, we used torin1, a potent ATP competitive inhibitor of mTOR (Thoreen et al., 2009), as assessed by the dephosphorylation of the mTOR substrate 4EBP1 (Fig. 8, d and e). Torin1 treatment of *Tsc2*^{-/-} MEFs promoted LC3 lipidation, indicating an induction of the autophagic flux, which was accompanied by a reduction of YAP levels (Fig. 8 d). The effect of Torin1 was also observed in autophagy-competent control MEFs (Fig. 8, d and e). However, in autophagy deficient *Atg7*^{-/-} MEFs, mTOR inhibition was largely unable to induce YAP degradation (Fig. 8 e). Similar to Torin1 treatment, nutrient starvation also promoted YAP degradation concomitantly with the induction of autophagy in a chloroquine-sensitive manner (Fig. 8 f). Of note, ectopic Flag-YAP co-immunoprecipitated with the autophagy cargo receptor p62 and with the upstream kinase Lats1 in basal conditions (Fig. 8 g). Upon autophagy induction by nutrient starvation together with chloroquine treatment to induce a late autophagy block, the interaction with p62 and Lats1 was, respectively, up- and down-regulated. Finally, the in vivo deletion of *Atg7* in epithelial cells of kidney proximal tubules was sufficient to cause the accumulation of YAP in lysates from the whole mouse kidneys (Fig. 8 h). In conclusion, mTOR regulates YAP degradation through autophagy, which is dependent on ATG7. Our data favor a model in which the control of YAP lysosomal degradation by mTOR matches YAP activity with nutrient availability in growth permissive conditions.

DISCUSSION

We delineate a crosstalk between two master regulators of growth, mTOR and YAP. Mechanistically, the impairment of autophagy, a result of mTOR hyperactivity in TSC1/2 mutant cells, leads to the accumulation of the oncogene YAP. The consequence is the establishment of the growth-promoting YAP transcriptional program, thus defining a novel protumoral target downstream of mTOR. By establishing a novel multisystem mouse model of TSC and by screening human TSC samples, we reveal that this molecular mechanism is required for the tumorigenesis of TSC-related kidney lesions and in PEComas.

Rapamycin derivatives (rapalogs) are approved for the treatment of TSC lesions, including subependymal giant cell astrocytomas, angiomyolipomas, and lymphangioliomyomatosis (Bissler et al., 2013; Franz et al., 2013). In many cases, these allosteric inhibitors of mTOR constituted a major improvement in the management of the disease. However, long term administration of rapalogs may have undesirable side effects, including dislipidemia, hyperglycemia, stomatitis, skin rash, lung fibrosis, leucopenia, and anemia. Our data suggest that preclinical trials targeting the YAP pathway, alone or in combination with rapalogs, should be considered for TSC, as they may limit the adverse effects. Importantly, a large variety of G protein-coupled receptors (GPCRs) have been recently identified as positive and negative up-stream regulators of the Hippo-YAP pathway (Yu et al., 2012). Future studies should define the GPCR present in the different TSC lesions and test their activity on YAP. Pharmacological agents acting on the angiotensin and adrenergic GPCR are well tolerated and have interesting actions that should be considered in this scenario. Angiotensin antagonists ameliorate renal injury in conditions of hypertension and fibrosis (Remuzzi et al., 2002). Propranolol, a β adrenergic antagonist, has striking efficacy against infantile hemangioma, possibly due to inhibition of angiogenesis and pericyte functions (Léauté-Labrèze et al., 2008). Whether these agents act on YAP and are effective against TSC PEComas are remarkable possibilities to explore.

MATERIALS AND METHODS

Mice. *Tsc1*^{fl/fl} and *CAGGCre-ER* mice were obtained from The Jackson Laboratory. *Yap*^{fl/fl} mice were previously described (Xin et al., 2011). R26-floxstop-LacZ mice were obtained from C. Colnot (Institut Imagine, Paris, France). *Yap*^{+/+} and *Yap*^{+/-} mice were shared by U. Apte. Kidney-proximal tubule-specific *Atg7* knockout mouse samples, using a modified PEPCK-driven Cre, were provided by Z. Dong. All animal studies were approved by the Direction Départementale des Services Vétérinaires (Préfecture de Police, Paris, France; authorization number 75-1313) and the ethical committee of Paris Descartes University. Mice were housed in a 12-h light/dark cycle and fed a standard chow. All mice used in this study were on mixed genetic background (C57BL/6J, BALB/cJ, or 129/SvJae), with control mice being Cre-negative littermates of mutant mice. Female mice were used unless otherwise indicated. Tamoxifen (Sigma-Aldrich) dissolved in corn oil (Sigma-Aldrich; 10 mg/ml) was injected i.p. into pregnant females with a dose of 10 mg/kg at E15.5 (the day of vaginal plug observed was considered as E0.5). 1 mg/ml tamoxifen prepared in corn oil was used to inject subcutaneously the pups (10 mg/kg) at postnatal day 2 to generate mosaic-*Tsc1KO*; *Yap*^{+/-}. Blood was collected using tubes with EDTA (KABE LABORTECHNIK)

centrifuged at 500 g for 3 min. Plasma was isolated and analyzed for urea levels with an AU400 instrument (Olympus).

Human TSC samples. Human samples were retrieved from the files of the Department of Pathology and Diagnostics of the University of Verona and from Institut Bergonié of Bordeaux. The frozen samples included five angiomyolipoma samples and two resected kidney samples as consequences of TSC-unrelated diseases, pyelonephritis, or oncocytoma. Paraffin-embedded human PEComa samples included seven angiomyolipomas, two lymphangiomyomatosis, and one hepatic angiomyolipoma. Human studies were ethically approved by the Comité de Protection des Personnes (CPP Ile de France III) with the reference file #AT144.

Cell culture and reagents. HEK293, *Tsc2^{+/+};p53^{-/-}*, and *Tsc2^{-/-};p53^{-/-}* MEFs were cultured in DMEM with 10% FBS, 1% penicillin/streptomycin. *Atg7^{+/+}* and *Atg7^{-/-}* MEFs were provided by M. Komatsu (Tokyo Metropolitan Institute of Medical Science, Tokyo, Japan; Komatsu et al., 2005) and cultured in DMEM with 10% FBS, 1% nonessential amino acid (Invitrogen), 1% penicillin/streptomycin. All cells were cultured at 37°C and 5% CO₂. 5 × 10⁴ cells were seeded per well in a 6-well plate and cultured overnight before treatment with MG132 (Tocris), Chloroquine (Sigma-Aldrich), or Torin1 (Tocris). For RNAi experiments, 2 × 10⁴ HEK293 cells were seeded per well in a 6-well plate, cultured overnight, transfected with siRNAs targeting TSC1, TSC2, and ctrl siRNA (QIAGEN) using calcium phosphate method. 48 h later, second transfection with siRNAs was administered. Cells were harvested 96 h after the first siRNA transfection. MEFs were transfected with siCtrl and siYAP (Thermo Fisher Scientific) using DharmaFECT1 Transfection Reagent. For nutrient starvation, cells were cultured in EBSS (Invitrogen) for half an hour or 1 h. Flag-YAP plasmid was obtained from Addgene (#19045).

Immunohistochemistry and immunofluorescence. Mouse tissues were fixed in 4% paraformaldehyde, embedded in paraffin and sectioned at 4 μm. Sections were deparaffinized and hydrated before being incubated in citrate buffer (pH6) sub-boiling for 10 min. Sections were blocked in 3% Goat normal serum, 1% BSA and 0.1% Triton X-100 for 1 h, and then incubated with the following primary antibodies overnight at 4°C: anti-phospho-rpS6 (#5364), anti-Vimentin (#5741), anti-YAP (#4912), and anti-PDGFRβ (#3169; Cell Signaling Technology); anti-αSMA (#A2547; Sigma-Aldrich); anti-Ki67 (#PA5-19462; Thermo Fisher Scientific); anti-Pmel/HMB45 (#M0634; DAKO); anti-ICAM1 (#sc-107; Santa Cruz Biotechnology, Inc.); anti-H-caldesmon (#ab50016), anti-CD31 (#ab28364), anti-Pmel (#ab137078), anti-Cathepsin K (#ab19027), and anti-β-gal (#ab9361; Abcam). Next, sections were incubated with biotinylated secondary antibodies, detected with Vectastain Elite ABC kit (Vector) and DAB chromogen system (DAKO). For immunofluorescence, Alexa Fluor 488- or Alexa Fluor 568-conjugated secondary antibodies (Molecular Probes) were used and DNA was stained by DAPI within the mounting medium (Vector Labs). For immunocytofluorescence, cells were grown on chamber slides (Millipore), fixed in 100% cold methanol, blocked in 3% goat normal serum, 1% BSA, and 0.1% Triton X-100/PBS, and incubated with the following antibodies: anti-YAP (#sc-101199; Santa Cruz Biotechnology, Inc.) and anti-Lamp2 (#ab13524; Abcam). Immunofluorescence slides were analyzed using an ApoTome2 microscope (Carl Zeiss). ImageJ software (National Institutes of Health) was used for quantification.

Immunoblotting and immunoprecipitation. Cells and tissues were lysed in cell lysis buffer (#9803; Cell Signaling Technology) with complete protease inhibitor cocktail and phosSTOP phosphatase inhibitor cocktail (Roche). Protein extracts were resolved by SDS-PAGE, transferred to PVDF membranes and incubated with the following primary antibodies: anti-αSMA (#A2547; Sigma-Aldrich); anti-Mart1 (#sc-20032; Santa Cruz Biotechnology, Inc.); anti-GAPDH (#ab9485), anti-CTGF (#ab6992; Abcam); anti-AREG (#sc-74501; Invitrogen); anti-TSC1 (#37-0400; Invitrogen);

anti-LC3 (#0231-100), anti-p62/SQSTM1 (#H00008878-M01; Abnova); anti-β-actin (#A5441), anti-α-tubulin (#T5168; Sigma-Aldrich); anti-YAP (#4912), anti-YAP/TAZ (#8418), anti-Lamin A/C (#2032), anti-rpS6 (#2217), anti-phospho-rpS6(Ser240/244; #5364), anti-p4EBP1(Thr37/46; #2855), anti-pYAP (Ser127; #4911), anti-Lats1 (#3477), anti-TSC2 (#4308), and anti-Ub (#3936; Cell Signaling Technology). Nuclear and cytoplasmic protein extractions were performed with NE-PER kit (#78835; Thermo Fisher Scientific). Flag-tagged YAP protein complex was immunoprecipitated from cell lysates with anti-Flag antibody (#F1804; Sigma-Aldrich) and protein G-Sepharose (#17-0618-01; GE Healthcare). Immunocomplexes were washed in cell lysis buffer three times and analyzed by immunoblotting.

BrdU labeling. Cells were incubated with 10 μg/ml BrdU (Sigma-Aldrich) for 3 h before harvest. Cells were washed, fixed in 4% paraformaldehyde for 15 min, incubated in citrate buffer (pH 6.0) at sub-boiling temperature, and detected with an anti-BrdU antibody (#11170376001; Roche). The percentage of BrdU incorporation was determined by counting BrdU⁺ nuclei among at least 200 cells in distinct fields. For in vivo studies, mice were injected i.p. with BrdU (50 mg/kg) for 24 h before sacrifice.

TUNEL assay. TUNEL assays were performed using In Situ Cell Death Detection kit (Roche) according to the manufacturer's instructions.

Temsirolimus and verteporfin treatments. Temsirolimus (LC Laboratories) was dissolved in 100% ethanol (25 mg/ml), aliquoted, and stored at -20°C. 1 mg/ml working solution was prepared in 5% Tween-80, 5% PEG400, and 86% PBS before injection. Mice were injected i.p. with vehicle or temsirolimus (5 mg/kg) every other day for 2 wk. Verteporfin (Selleckchem) was dissolved in DMSO (100 mg/ml), aliquoted, and stored at -80°C. Working solution was prepared at 10 mg/ml in PBS freshly before use. Mice were administered i.p. with vehicle or verteporfin solution at a dose of 100 mg/kg every other day for 10 d. In vitro, cells were treated with DMSO or verteporfin with a dose of 4 μM.

Quantitative RT-PCR. Total RNA was extracted from tissue or cells using an RNeasy Mini kit (QIAGEN), following the manufacturer's instructions. Single-strand cDNA was synthesized from 1 μg of total RNA with SuperScript II (Invitrogen) and random hexamer primers. Real-time quantitative PCR was performed on MX3005P instrument (Agilent) using a Brilliant III SYBR Green QPCR Master Mix (Agilent). Relative amounts of the indicated mRNAs were determined by means of the 2^{-ΔΔCT} method, normalizing with β-actin levels. The primer sequences used were mouse β-actin, 5'-GTGACGTTGACATCCGTAAGA-3' and 5'-GCCGGA-CTCATCGTACTCC-3'; mouse Mart1, 5'-TCCCAGGAAGGGGCACAGACG-3' and 5'-AGCGTTGGGAACCCAGGGCT-3'; mouse Cathepsin K, 5'-AAGTGGTTCAGAGATGACGGGAC-3' and 5'-TCTTCAGAGTCAATGCCTCCGTTCC-3'; mouse Pmel, 5'-TGACGGTGGACCCTGCCCAT-3' and 5'-AGCTTTGCGTGGCCCGTAGC-3'; mouse Tyrp1, 5'-CCCTAGCCTATATCTCCCTTTT-3' and 5'-TACCATCGTGGGGA-TAATGGC-3'; mouse Yap, 5'-GTCCTCCTTTGAGATCCCTGA-3' and 5'-TGTTGTGTCTGATCGTTGTGAT-3'; mouse Ctgf, 5'-GTGC-CAGAAGCCACTG-3' and 5'-CCCCGGTTACTACTCAA-3'; mouse Cyr61, 5'-GGATCTGTGAAGTGCCTCT-3' and 5'-CTGCA-TTTCTTGCCCTTTT-3'; mouse Areg, 5'-TCATGGCGAATGCA-GATACA-3' and 5'-GCTACTACTGCAATCTTGA-3'; mouse Hes1, 5'-GGAGAGGCTGCCAAGGTTTT-3' and 5'-GCAAATGGCCGT-CAGGA-3'; mouse Hes5, 5'-TCTCCACGATGATCCTTAAAGGA-3' and 5'-CAAATCGTGCCACATGC-3'; mouse Cdx1, 5'-TTCACACAGCCGGTACATCA-3' and 5'-GCCAGCATTAG-TAGGGCATAGA-3'; mouse Fgf4, 5'-TGCCTTTCTTTACCGAC-GAGT-3' and 5'-GCGTAGGATTCGTAGGCGTT-3'; mouse Gli1, 5'-CATCCACAGGACAGCTCAA-3' and 5'-TGGCAGGGCTCT-GACTAACT-3'; mouse Gli2, 5'-CCTTCTCCAATGCCTCAGAC-3' and 5'-GGGTCTGTGTACCTCTGG-3'.

Statistical analysis. Data are shown as means \pm SEM. Analysis was performed by unpaired, two-tailed, Student's *t* test unless otherwise indicated. $P < 0.05$ was considered statistically significant.

We are grateful to the members of Institut National de la Santé et de la Recherche Médicale-U1151 for support, to Masaaki Komatsu and Jean Michel Coindre for sharing reagents, and to Stefano Fumagalli, Patrice Codogno, Nicolas Dupont, and to Mustafa Sahin for critically reading the manuscript. We thank Sophie Berissi and Nicolas Goudin for the technical help.

This work was supported by grants from the European Research Council, Fondation de la Recherche Médicale, Fondation Schlumberger pour l'Éducation et la Recherche, Institut National du Cancer, Association Sclérose Tubéreuse de Bourneville, the Association pour la Recherche sur le Cancer, Contrat d'interface avec l'Hôpital to M. Pende. N. Liang received a fellowship from the China Scholarship Council and Association pour la Recherche sur le Cancer.

The authors have declared that no conflict of interest exists.

Submitted: 19 February 2014

Accepted: 27 August 2014

REFERENCES

- Bissler, J.J., J.C. Kingswood, E. Radzikowska, B.A. Zonnenberg, M. Frost, E. Belousova, M. Sauter, N. Nonomura, S. Brakemeier, P.J. de Vries, et al. 2013. Everolimus for angioleiomyoma associated with tuberous sclerosis complex or sporadic lymphangiomyomatosis (EXIST-2): a multicentre, randomised, double-blind, placebo-controlled trial. *Lancet*. 381:817–824. [http://dx.doi.org/10.1016/S0140-6736\(12\)61767-X](http://dx.doi.org/10.1016/S0140-6736(12)61767-X)
- Brittle, A.L., A. Repiso, J. Casal, P.A. Lawrence, and D. Strutt. 2010. Four-jointed modulates growth and planar polarity by reducing the affinity of dachsous for fat. *Curr. Biol.* 20:803–810. <http://dx.doi.org/10.1016/j.cub.2010.03.056>
- Calvo, E., N. Ege, A. Grande-García, S. Hooper, R.P. Jenkins, S.I. Chaudhry, K. Harrington, P. Williamson, E. Moeendarbary, G. Charras, and E. Sahai. 2013. Mechanotransduction and YAP-dependent matrix remodelling is required for the generation and maintenance of cancer-associated fibroblasts. *Nat. Cell Biol.* 15:637–646. <http://dx.doi.org/10.1038/ncb2756>
- Camargo, F.D., S. Gokhale, J.B. Jhonnidid, D. Fu, G.W. Bell, R. Jaenisch, and T.R. Brummelkamp. 2007. YAP1 increases organ size and expands undifferentiated progenitor cells. *Curr. Biol.* 17:2054–2060. <http://dx.doi.org/10.1016/j.cub.2007.10.039>
- Choi, A.M., S.W. Ryter, and B. Levine. 2013. Autophagy in human health and disease. *N. Engl. J. Med.* 368:651–662. <http://dx.doi.org/10.1056/NEJMr1205406>
- Cordenonsi, M., F. Zanconato, L. Azzolin, M. Forcato, A. Rosato, C. Frasson, M. Inui, M. Montagner, A.R. Parenti, A. Poletti, et al. 2011. The Hippo transducer TAZ confers cancer stem cell-related traits on breast cancer cells. *Cell*. 147:759–772. <http://dx.doi.org/10.1016/j.cell.2011.09.048>
- Crino, P.B., K.L. Nathanson, and E.P. Henske. 2006. The tuberous sclerosis complex. *N. Engl. J. Med.* 355:1345–1356. <http://dx.doi.org/10.1056/NEJMr055323>
- Dibble, C.C., W. Elis, S. Menon, W. Qin, J. Klekota, J.M. Asara, P.M. Finan, D.J. Kwiatkowski, L.O. Murphy, and B.D. Manning. 2012. TBC1D7 is a third subunit of the TSC1-TSC2 complex upstream of mTORC1. *Mol. Cell*. 47:535–546. <http://dx.doi.org/10.1016/j.molcel.2012.06.009>
- Dong, J., G. Feldmann, J. Huang, S. Wu, N. Zhang, S.A. Comerford, M.F. Gayyed, R.A. Anders, A. Maitra, and D. Pan. 2007. Elucidation of a universal size-control mechanism in *Drosophila* and mammals. *Cell*. 130:1120–1133. <http://dx.doi.org/10.1016/j.cell.2007.07.019>
- Franz, D.N., E. Belousova, S. Sparagana, E.M. Bebin, M. Frost, R. Kuperman, O. Witt, M.H. Kohrman, J.R. Flamini, J.Y. Wu, et al. 2013. Efficacy and safety of everolimus for subependymal giant cell astrocytomas associated with tuberous sclerosis complex (EXIST-1): a multicentre, randomised, placebo-controlled phase 3 trial. *Lancet*. 381:125–132. [http://dx.doi.org/10.1016/S0140-6736\(12\)61134-9](http://dx.doi.org/10.1016/S0140-6736(12)61134-9)
- Halder, G., and R.L. Johnson. 2011. Hippo signaling: growth control and beyond. *Development*. 138:9–22. <http://dx.doi.org/10.1242/dev.045500>
- Halder, G., S. Dupont, and S. Piccolo. 2012. Transduction of mechanical and cytoskeletal cues by YAP and TAZ. *Nat. Rev. Mol. Cell Biol.* 13:591–600. <http://dx.doi.org/10.1038/nrm3416>
- Hayashi, S., and A.P. McMahon. 2002. Efficient recombination in diverse tissues by a tamoxifen-inducible form of Cre: a tool for temporally regulated gene activation/inactivation in the mouse. *Dev. Biol.* 244:305–318. <http://dx.doi.org/10.1006/dbio.2002.0597>
- He, C., and D.J. Klionsky. 2009. Regulation mechanisms and signaling pathways of autophagy. *Annu. Rev. Genet.* 43:67–93. <http://dx.doi.org/10.1146/annurev-genet-102808-114910>
- Huang, J., S. Wu, J. Barrera, K. Matthews, and D. Pan. 2005. The Hippo signaling pathway coordinately regulates cell proliferation and apoptosis by inactivating Yorkie, the *Drosophila* Homolog of YAP. *Cell*. 122:421–434. <http://dx.doi.org/10.1016/j.cell.2005.06.007>
- Kobayashi, T., O. Minowa, Y. Sugitani, S. Takai, H. Mitani, E. Kobayashi, T. Noda, and O. Hino. 2001. A germ-line Tsc1 mutation causes tumor development and embryonic lethality that are similar, but not identical to, those caused by Tsc2 mutation in mice. *Proc. Natl. Acad. Sci. USA*. 98:8762–8767. <http://dx.doi.org/10.1073/pnas.151033798>
- Komatsu, M., S. Waguri, T. Ueno, J. Iwata, S. Murata, I. Tanida, J. Ezaki, N. Mizushima, Y. Ohsumi, Y. Uchiyama, et al. 2005. Impairment of starvation-induced and constitutive autophagy in Atg7-deficient mice. *J. Cell Biol.* 169:425–434. <http://dx.doi.org/10.1083/jcb.200412022>
- Kwon, Y., A. Vinayagam, X. Sun, N. Dephoure, S.P. Gygi, P. Hong, and N. Perrimon. 2013. The Hippo signaling pathway interactome. *Science*. 342:737–740. <http://dx.doi.org/10.1126/science.1243971>
- Laplanche, M., and D.M. Sabatini. 2012. mTOR signaling in growth control and disease. *Cell*. 149:274–293. <http://dx.doi.org/10.1016/j.cell.2012.03.017>
- Léauté-Labrèze, C., E. Dumas de la Roque, T. Hubiche, F. Boralevi, J.B. Thambo, and A. Taïeb. 2008. Propranolol for severe hemangiomas of infancy. *N. Engl. J. Med.* 358:2649–2651. <http://dx.doi.org/10.1056/NEJMc0708819>
- Liu-Chittenden, Y., B. Huang, J.S. Shim, Q. Chen, S.J. Lee, R.A. Anders, J.O. Liu, and D. Pan. 2012. Genetic and pharmacological disruption of the TEAD-YAP complex suppresses the oncogenic activity of YAP. *Genes Dev.* 26:1300–1305. <http://dx.doi.org/10.1101/gad.192856.112>
- Manning, B.D., and L.C. Cantley. 2003. Rheb fills a GAP between TSC and TOR. *Trends Biochem. Sci.* 28:573–576. <http://dx.doi.org/10.1016/j.tics.2003.09.003>
- Martignoni, G., M. Pea, D. Reghellin, G. Zamboni, and F. Bonetti. 2008. PEComas: the past, the present and the future. *Virchows Arch.* 452:119–132. <http://dx.doi.org/10.1007/s00428-007-0509-1>
- McCormack, F.X., Y. Inoue, J. Moss, L.G. Singer, C. Strange, K. Nakata, A.F. Barker, J.T. Chapman, M.L. Brantly, J.M. Stocks, et al. National Institutes of Health Rare Lung Diseases Consortium/MILES Trial Group. 2011. Efficacy and safety of sirolimus in lymphangiomyomatosis. *N. Engl. J. Med.* 364:1595–1606. <http://dx.doi.org/10.1056/NEJMoa1100391>
- Meikle, L., D.M. Talos, H. Onda, K. Pollizzi, A. Rotenberg, M. Sahin, F.E. Jensen, and D.J. Kwiatkowski. 2007. A mouse model of tuberous sclerosis: neuronal loss of Tsc1 causes dysplastic and ectopic neurons, reduced myelination, seizure activity, and limited survival. *J. Neurosci.* 27:5546–5558. <http://dx.doi.org/10.1523/JNEUROSCI.5540-06.2007>
- Mizushima, N., and M. Komatsu. 2011. Autophagy: renovation of cells and tissues. *Cell*. 147:728–741. <http://dx.doi.org/10.1016/j.cell.2011.10.026>
- Onda, H., A. Lueck, P.W. Marks, H.B. Warren, and D.J. Kwiatkowski. 1999. Tsc2(+/-) mice develop tumors in multiple sites that express gelsolin and are influenced by genetic background. *J. Clin. Invest.* 104:687–695. <http://dx.doi.org/10.1172/JCI7319>
- Pan, D. 2010. The Hippo signaling pathway in development and cancer. *Dev. Cell*. 19:491–505. <http://dx.doi.org/10.1016/j.devcel.2010.09.011>
- Parkhitko, A., F. Myachina, T.A. Morrison, K.M. Hindi, N. Auricchio, M. Karbowiczek, J.J. Wu, T. Finkel, D.J. Kwiatkowski, J.J. Yu, and E.P. Henske. 2011. Tumorigenesis in tuberous sclerosis complex is autophagy and p62/sequestosome 1 (SQSTM1)-dependent. *Proc. Natl. Acad. Sci. USA*. 108:12455–12460. <http://dx.doi.org/10.1073/pnas.1104361108>
- Remuzzi, G., P. Ruggenenti, and N. Perico. 2002. Chronic renal diseases: renoprotective benefits of renin-angiotensin system inhibition. *Ann. Intern. Med.* 136:604–615. <http://dx.doi.org/10.7326/0003-4819-136-8-200204160-00010>

- Tapon, N., and K.F. Harvey. 2012. The Hippo pathway—from top to bottom and everything in between. *Semin. Cell Dev. Biol.* 23:768–769. <http://dx.doi.org/10.1016/j.semcdb.2012.08.007>
- Thoreen, C.C., S.A. Kang, J.W. Chang, Q. Liu, J. Zhang, Y. Gao, L.J. Reichling, T. Sim, D.M. Sabatini, and N.S. Gray. 2009. An ATP-competitive mammalian target of rapamycin inhibitor reveals rapamycin-resistant functions of mTORC1. *J. Biol. Chem.* 284:8023–8032. <http://dx.doi.org/10.1074/jbc.M900301200>
- Tumaneng, K., R.C. Russell, and K.L. Guan. 2012. Organ size control by Hippo and TOR pathways. *Curr. Biol.* 22:R368–R379. <http://dx.doi.org/10.1016/j.cub.2012.03.003>
- Xin, M., Y. Kim, L.B. Sutherland, X. Qi, J. McAnally, R.J. Schwartz, J.A. Richardson, R. Bassel-Duby, and E.N. Olson. 2011. Regulation of insulin-like growth factor signaling by Yap governs cardiomyocyte proliferation and embryonic heart size. *Sci. Signal.* 4:ra70.
- Yu, F.X., and K.L. Guan. 2013. The Hippo pathway: regulators and regulations. *Genes Dev.* 27:355–371. <http://dx.doi.org/10.1101/gad.210773.112>
- Yu, F.X., B. Zhao, N. Panupinthu, J.L. Jewell, I. Lian, L.H. Wang, J. Zhao, H. Yuan, K. Tumaneng, H. Li, et al. 2012. Regulation of the Hippo-YAP pathway by G-protein-coupled receptor signaling. *Cell.* 150:780–791. <http://dx.doi.org/10.1016/j.cell.2012.06.037>
- Zhang, H., G. Cicchetti, H. Onda, H.B. Koon, K. Asrican, N. Bajraszewski, F. Vazquez, C.L. Carpenter, and D.J. Kwiatkowski. 2003. Loss of Tsc1/Tsc2 activates mTOR and disrupts PI3K-Akt signaling through down-regulation of PDGFR. *J. Clin. Invest.* 112:1223–1233. <http://dx.doi.org/10.1172/JCI200317222>
- Zhao, B., X. Wei, W. Li, R.S. Udan, Q. Yang, J. Kim, J. Xie, T. Ikenoue, J. Yu, L. Li, et al. 2007. Inactivation of YAP oncoprotein by the Hippo pathway is involved in cell contact inhibition and tissue growth control. *Genes Dev.* 21:2747–2761. <http://dx.doi.org/10.1101/gad.1602907>
- Zhao, B., X. Ye, J. Yu, L. Li, W. Li, S. Li, J. Yu, J. D. Lin, C. Y. Wang, A. M. Chinnaiyan, et al. 2008. TEAD mediates YAP-dependent gene induction and growth control. *Genes Dev.* 22:1962–1971. <http://dx.doi.org/10.1101/gad.1664408>
- Zhao, B., L. Li, K. Tumaneng, C.Y. Wang, and K.L. Guan. 2010. A coordinated phosphorylation by Lats and CK1 regulates YAP stability through SCF(beta-TRCP). *Genes Dev.* 24:72–85. <http://dx.doi.org/10.1101/gad.1843810>
- Zhou, J., J. Brugarolas, and L.F. Parada. 2009. Loss of Tsc1, but not Pten, in renal tubular cells causes polycystic kidney disease by activating mTORC1. *Hum. Mol. Genet.* 18:4428–4441. <http://dx.doi.org/10.1093/hmg/ddp398>
- Zhou, J., G. Shrikhande, J. Xu, R.M. McKay, D.K. Burns, J.E. Johnson, and L.F. Parada. 2011. Tsc1 mutant neural stem/progenitor cells exhibit migration deficits and give rise to subependymal lesions in the lateral ventricle. *Genes Dev.* 25:1595–1600. <http://dx.doi.org/10.1101/gad.16750211>